PVP2020-21708

TEMPERING EFFICIENCY EVALUATION FOR DISSIMILAR WELD OVERLAYS

Eun Jang[1], Jeffrey Stewart[1], Yuxiang Luo[1], Shijie Qu[1], Dr. Boian Alexandrov[1],
Steven L. McCracken[2], Jonathan Tatman[2], Dr. Darren Barborak[3], Dr. Jorge A. Penso[4]

[1]The Ohio State University, Columbus, OH; [2]EPRI Welding and Repair Technology Center, Charlotte, NC;
[3]AZZ Specialty Welding, Atlanta, GA; [4]Shell Global Solutions (US), Inc., Houston, TX, USA

ABSTRACT

The objective of this work was to develop a procedure for evaluation and quantification of the tempering efficiency of corrosion resistant weld overlays used in the power generation and oil and gas industries. Three two-layer weld overlays of Alloy 625 on Grade 22 steel plates were produced using GTAW cold wire procedures. Typical welding parameters corresponding to low, medium, and high heat input were utilized. The overlays consisted of nine beads on the first layer and five to seven beads on the second layer. The weld thermal histories experienced in the coarse-grained heat affected zone (CGHAZ) were measured with Type K thermocouples and recorded with a 55 Hz sampling rate. Two rows of seven thermocouples were used in each overlay: one row located in a mid-bead position beneath the center bead of the overlay and the other row located in the nearest bead overlap position. Additionally, one Type C thermocouple was plunged into the weld pool of a second layer weld bead.

The acquired thermal histories and the CGHAZ hardness at the thermocouple locations were evaluated to quantify the tempering efficiency in each welding procedure. The weld thermal histories with peak temperatures between 500°C, assumed as the minimum tempering temperature, and the base metal A_{C1} temperature were considered as tempering thermal cycles. The number of tempering thermal cycles and the sum of tempering cycle's peak temperatures in each thermocouple location, as well as the corresponding hardness were used to quantify the tempering response efficiency for each of the three welding procedures. The results of this study will be used for validation of a computational model-based approach for prediction of tempering response and optimization of temper bead welding procedures.

NOMENCLATURE

MTT   minimum tempering temperature
SC   sub-critical HAZ

IC   inter-critical HAZ
FG   fine-grain HAZ
CG   coarse-grain HAZ
WM   weld metal
LHI   low heat input
MHI   medium heat input
HHI   high heat input
TC   thermocouple
WFS   wire feed speed

1. INTRODUCTION

When welding low alloy steels, there is often a need for post-weld heat treatment (PWHT) to temper brittle microstructures and relieve residual stresses in the base metal. During welding, part of the base metal HAZ reaches temperatures above A_{C1}, where austenite begins to form. Further heating past the A_{C3} temperature results in a full transformation to austenite. Rapid cooling rates from the austenite phase field leads to the formation of martensite in the HAZ, which is a hard and brittle microstructure. Martensite formation is a result of carbon being trapped in the austenitic matrix due to insufficient time allowed to diffuse out. Therefore, a PWHT is required to temper the HAZ by allowing some of the carbon in the martensite to diffuse out and form carbides [1].

PWHT is performed to elevate the temperature of the weldment below the A_{C1} temperature. Staying below A_{C1} ensures that no re-transformation to austenite will occur, which erases any previous tempering cycles. Commonly, a furnace has been used to perform PWHT. However, using a furnace for PWHT is not feasible in certain situations. These include large welds, which would not fit inside the furnace, as well as cladding or repair welds for already in-service components. These issues highlight the need for an alternative to PWHT such as temper bead welding.

Temper bead welding is a process which uses adjacent weld beads to temper the previous beads in the overlay. Moreover, an additional layer of beads can be welded on top of the first layer to provide additional tempering to the base metal HAZ. Figure 1 below gives an illustration of temper bead welding with two weld layers.
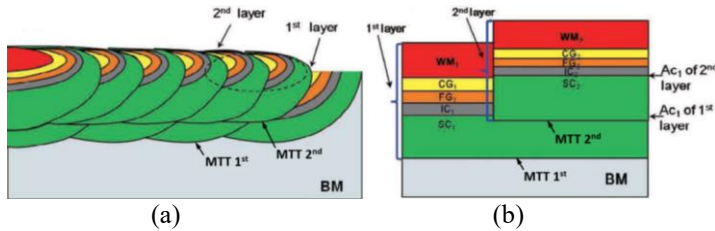

Figure 1: Schematic of temper bead weld zones: (a) Overlapping beads. (b) Regions of the HAZ generated. Modified from Yu et. al. [2]

Temper bead welding techniques are often developed by a trial-and-error approach where welding procedures must be qualified by hardness and/or Charpy V-notch impact testing [3]. In an effort to optimize qualification of temper bead procedures, Forquer and Stewart, developed a method for quantification of temper bead tempering efficiency to output response variables based on the thermal history [5, 6]. In addition, Stewart developed an approach to predict the HAZ hardness using one of the response variables taken from the thermal history [4, 5]. This study will attempt to validate the approach for quantification of tempering response in temper bead welding by performing hardness tests and analyzing thermal histories in experimental weld overlays.

2. MATERIALS AND METHODS

Three weld overlays were made with Alloy 625 (ERNiCrMo-3) filler metal on ASTM A-387 Grade 22 steel plate using the cold wire gas tungsten arc welding (GTAW) process. The Alloy 625 filler metal was 0.045 in. (1.14mm) diameter and the Grade 22 steel plates had dimensions of 6 in. x 8 in. x 1 in. (152mm x 203mm x 25mm). Compositions for the filler metal and plate are shown in Table 1.

Three sets of welding parameters, corresponding to low, medium, and high heat input (LHI, MHI, and HHI) were used in this study to produce two-layer overlays as shown in Table 2.

The MHI set of parameters is typically used for weld overlays, while the LHI and HHI would not be commonly seen in industry practice but offer distinct differences in bead-shape and expected tempering efficiency.

Initially, the three sets of parameters were used to produce single-layer five-bead overlays, as shown in Figure 2. These overlays were cross-sectioned for measurement of single- and multi-bead geometries, as well as bead overlap and mid-bead spacing distances. The bead penetration and spacing distances were needed to determine thermocouple locations for accurate measurements of HAZ thermal histories at bead overlap and mid-bead locations.

Table 1: Chemical composition of A-387 Grade 22 steel plate and Alloy 625 filler metal, wt.%.

	A-387 Gr 22	Alloy 625
Fe	Bal.	0.23
C	0.13	0.01
Mn	0.52	0.04
Cr	2.25	22.23
Mo	0.94	8.61
Cu	0.17	0.03
Si	0.21	0.04
Ni	0.12	64.7
Al	0.033	0.1
Nb	0.001	3.59
Co	-	0.01
Ti	0.003	0.21
B	0.0001	-
P	0.016	0.003
S	0.009	0.001

Table 2: Weld overlay parameters

Welding Parameters				
HI	**Parameter**	**Value**	**# Beads Layer 1**	**# Beads Layer 2**
LHI	Current	156 A	9	5
	Voltage	10.1 V		
	Travel	2.5 in/min (6.35 cm/min)		
	WFS	27 in/min (68.6 cm/min)		
MHI	Current	212 A	9	7
	Voltage	11 V		
	Travel	2.6 in/min (6.60 cm/min)		
	WFS	38 in/min (96.5 cm/min)		
HHI	Current	260A	9	5
	Voltage	11.4V		
	Travel	1.95 in/min (4.95 cm/min)		
	WFS	41 in/min (104 cm/min)		

Figure 2: Test overlays used to determine TC placement.

Each of the three plates used for the two-layer overlays was instrumented with fourteen Type K thermocouples (TC). Thermocouples TC 1 through TC 7 were located along the overlap position of beads #3 and #4 in the first layer. TC 7 through TC 14 were positioned along the maximum penetration (mid-bead position) of bead #5. The thermocouples were located at varying distance from the fusion boundary, aiming to capture the thermal histories throughout the HAZ and equally spaced along the plate length. The distances of thermocouple hole tips to the plate top surfaces for the three plates are listed in Table 3. The location of the thermocouples relative to the weld beads can be seen in Figure 3.

The Type K thermocouple wires were installed into ceramic insulators, their tips welded together, inserted into the plate holes, and welded to the plate tips using a capacitor discharge welder. Following welding, the holes were filled in with epoxy resin to hold the thermocouples in place.

The LHI, MHI, and HHI two-layer weld overlays were produced on the thermocouple-instrumented plates using the parameters listed in Table 2. An example of a completed two-layer overlay is shown in Figure 4. During welding, the thermocouple signals were recorded using two Instrunet 100 data acquisition systems at 55 Hz frequency and two personal computers.

The thermocouple data was processed with a MatLab script to determine the maximum temperatures, heating and cooling rates of the thermal histories recorded by each thermocouple. A methodology for quantification of tempering response in multipass welding, developed by Stewart and Alexandrov [4], was applied to predict the HAZ hardness resulting from the multiple reheats in the three weld overlays. That methodology is based on calculation of an equivalent Grange-Baughman Parameter (GBP) for weld thermal histories with multiple reheats and on experimentally developed relationships between GBP and the resulting hardness. The GBP value makes use of the

Holloman Jaffe equation to quantify the effects of alloying elements on hardness after tempering treatments [5]. Equations (1) and (2) shown below were developed for the tested heat of Grade 22 steel [4]. These equations were used for hardness prediction at the thermocouple locations of the three test plates.

$$CGHAZ\ Hardness\ (HV) = -1x10^{-6} * GBP^2 + 0.0393 * GBP + 18.783 \qquad [1]$$

$$ICHAZ\ Hardness\ (HV) = -6x10^{-7} * GBP^2 + 0.0243 * GBP + 53.335 \qquad [2]$$

Table 3: Distances of thermocouple hole tips from the plate's top surface.

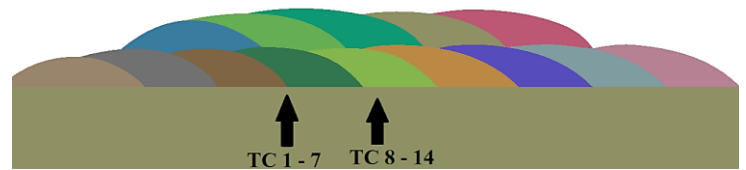| LHI		MHI		HHI	
Hole #	Distance, mm	Hole #	Distance, mm	Hole #	Distance mm
1	0.2	1	0.4	1	0.5
2	0.4	2	0.6	2	0.7
3	0.6	3	0.8	3	0.9
4	0.8	4	1.0	4	1.1
5	1.0	5	1.2	5	1.3
6	1.2	6	1.4	6	1.5
7	1.5	7	1.6	7	1.7
8	0.6	8	0.8	8	0.9
9	0.7	9	0.9	9	1.0
10	0.8	10	1.0	10	1.1
11	0.9	11	1.1	11	1.2
12	1.1	12	1.3	12	1.4
13	1.3	13	1.5	13	1.6
14	1.5	14	1.7	14	1.8

Figure 3: Location of thermocouples during experimental welding. Two rows (TC 1-7 is between 3/4th bead interbead, and TC 8-14 is beneath the 5th bead, midbead).

Figure 4: Completed two-layer weld overlay using the HHI welding parameters.

3. RESULTS AND DISCUSSION

Typical thermal histories recorded at HAZ bead overlap and mid-bead positions are shown in Figures 5 through 10. The A_{C1}, A_{C3}, and the minimum tempering temperature (MTT) are also shown in these figures. MTT represents the lowest maximum temperature of a reheat thermal cycle that would provide a tempering effect on as-welded HAZ microstructures. These temperatures were experimentally determined for the tested heat of Grade 22 steel [5]. Previous research has shown that tempering effect in multipass welding is generated by multiple thermal cycles, named effective tempering cycles, with maximum temperatures between the A_{C1} and MTT temperatures. It was also found that the effective thermal cycle maximum temperature has the strongest effect on the tempering response. Reheating above the A_{C3} or A_{C1} will result in formation of fresh martensite on cooling, thus completely or partially erasing the tempering effects of previous reheats [5].

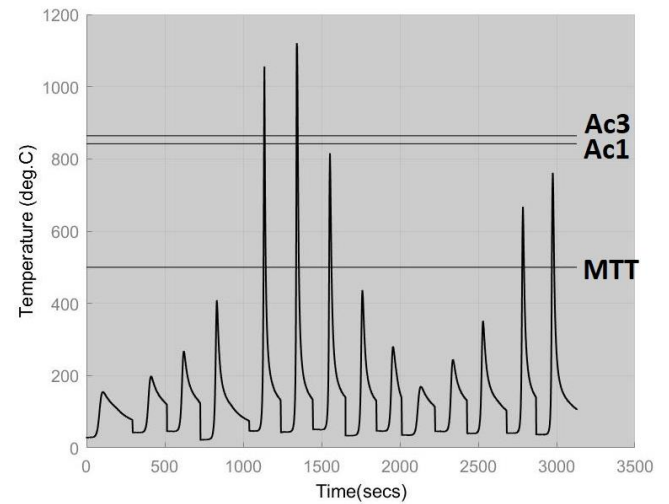**Figure 5:** Thermal history of TC 4 from the LHI plate

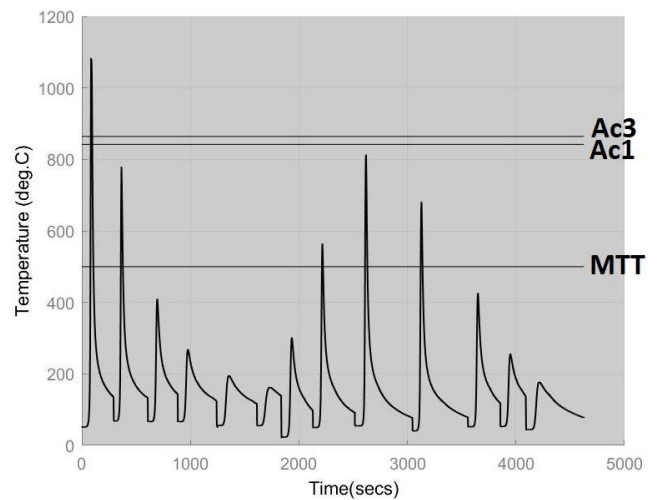**Figure 6:** Thermal history of TC 12 from the LHI plate.

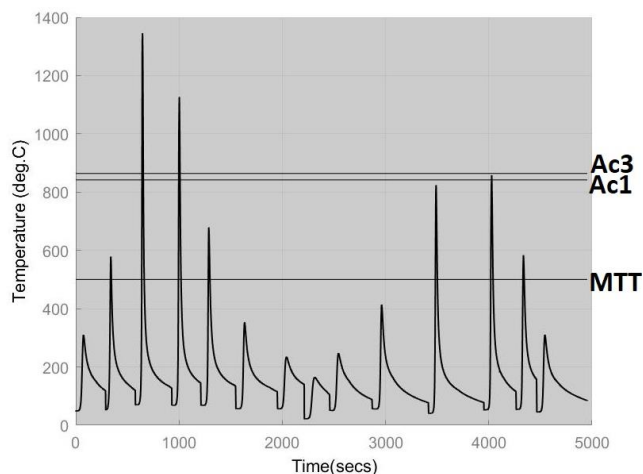**Figure 7:** Thermal history of TC 4 from the MHI plate.

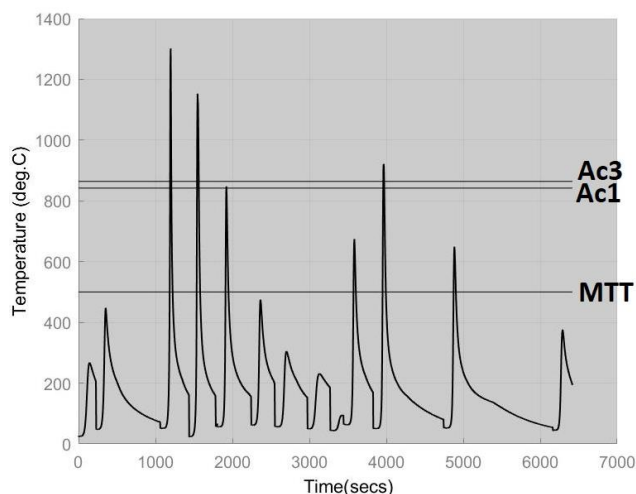**Figure 8:** Thermal history of TC 11 from the MHI plate.

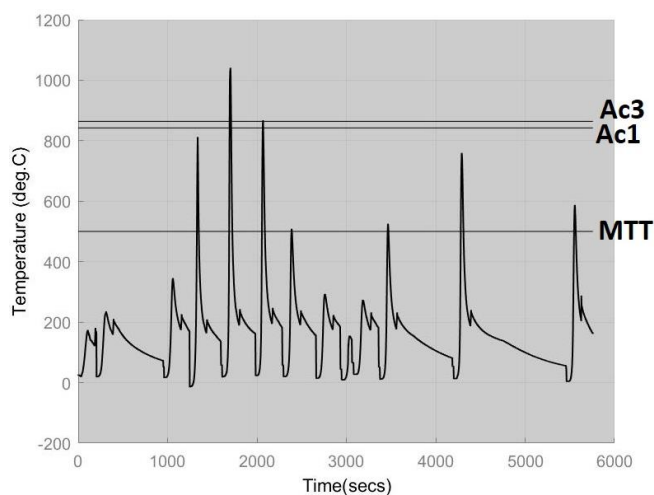**Figure 9:** Thermal history of TC 4 from the HHI plate

Figure 10: Thermal history of TC 11 from the HHI plate.

A previous study established the number of effective reheats (between the MTT and A_{C1}), the maximum temperature of experienced effective thermal cycles, the sum of effective thermal cycles maximum temperatures, the equivalent GBP, and the HAZ hardness as parameters for tempering efficiency evaluation [6]. The tempering efficiency parameters for the bead overlap and mid-bead positions with thermal histories shown in Figures 5 through 10 are summarized in Table 4. These results provided a general validation of the tempering efficiency quantification approach. Out of all CGHAZ TC locations, TC4 in the MHI procedure was subjected to the maximum tempering effect resulting from four tempering reheats, one from the first layer and three from the second layer, Figure 7. These generated the largest sum of effective reheat temperatures and largest corresponding GBP value, Table 4. The mid-bead location of TC 11 in the MHI procedure experienced two tempering reheats, one from the first layer and one from the second, that were partially erased by intercritical reheat from the second layer, Figure 8. Although this was only followed by one tempering reheat in the second layer, the entire thermal history in this ICHAZ location produced the lowest GBP value and lowest predicted hardness, Table 4.

As shown in Table 4, all mid-bead TC locations experienced greater tempering effect and had lower predicted hardness than the bead overlap locations for each heat input. This behavior can be analyzed with hardness maps overlaid on the two-layer macrographs in Figures 11 and 12. Each subsequent bead in the first layer tempers part of the previous bead HAZ, creating low hardness bands that are parallel to fusion boundary, Figures 11 and 12. However, the specific fusion boundary profile exposes the CGHAZ region of the bead-overlap locations to re-austenitization by the second layer reheats, erasing the tempering effect of the first layer overlapping beads, as shown in Figures 9, 11 and 12. In comparison, the deeper penetration at mid-bead locations prevents re-austenitization and allows for tempering reheats during the second layer deposition, Figures 9, 11 and 12.

Based on the TC locations listed in Table 4, the MHI procedure can be considered to be the most tempering efficient, followed by the LHI and HHI procedures. Complete tempering efficiency analysis for the tested WOL procedures will be performed after analyzing the tempering response in all TC locations.

Table 4: Tempering efficiency parameters for LHI TC 4 and 12, MHI TC 4 and 11, and HHI TC 4 and 11.

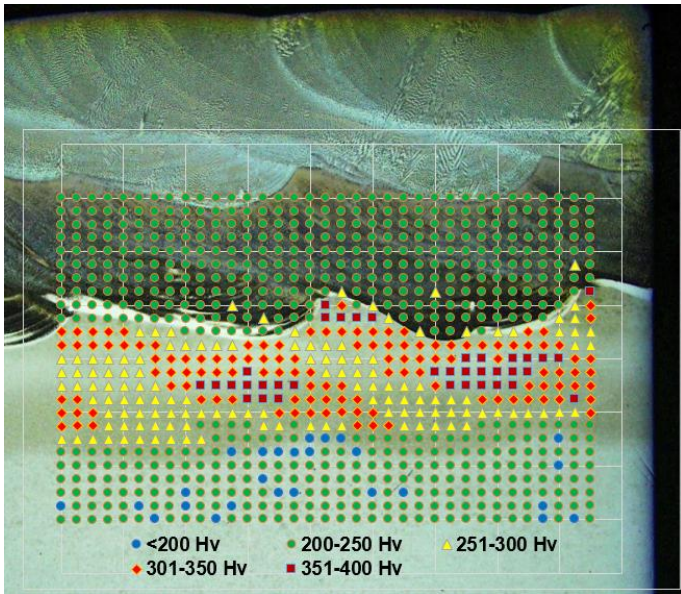| HI + TC	TC Location	Tempered Area	# Eff. Reheats	Max Eff. Reheat Temp.	Sum of Eff. Reheat Temp.	GBP	Pred. Hardness HV
LHI TC4	bead-overlap	CGHAZ	4	776.6	2597.1	2.85E+04	326
LHI TC12	mid-bead	CGHAZ	3	815.7	2244.6	2.96E+04	306
MHI TC4	bead-overlap	CGHAZ	4	813.3	2810.9	2.99E+04	299
MHI TC11	mid-bead	ICHAZ	1	584	584	2.35E+04	293
HHI TC4	bead-overlap	CGHAZ	1	649.2	649.2	2.57E+04	369
HHI TC11	mid-bead	CGHAZ	4	777.2	2401.6	2.86E+04	324

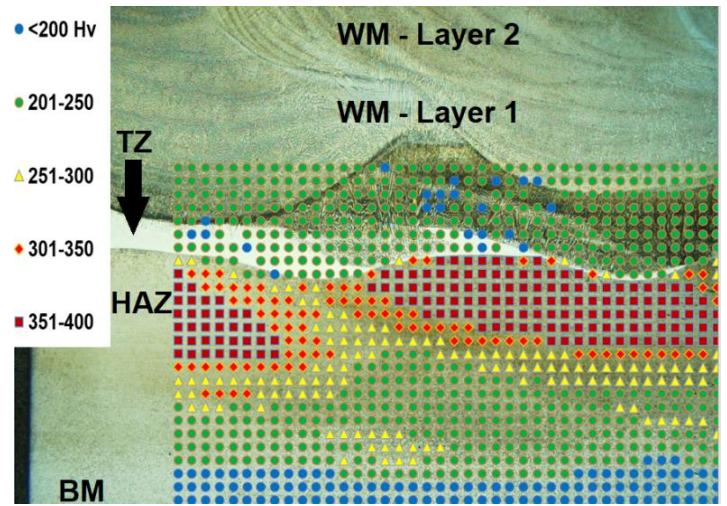**Figure 11:** Hardness map on LHI TC4 sample.

Figure 12: Hardness map on HHI TC4 sample.

The hardness maps in Figures 11 and 12 were developed in accordance with ASTM E384, with a load of 500g and indent spacing of 250 micrometers. These hardness maps provide overall validation of the tempering response prediction and tempering efficiency approaches developed by Stewart and Forquer [4, 5, 6]. The bead overlap locations in both hardness maps have higher hardness than the mid-bead locations and the bead overlap and mid-bead locations in the LHI procedure have lover hardness than the corresponding HHI locations, which correlates very well with the tempering efficiency and hardness predictions in Table 4.

Other welding procedure aspects that influence bead tempering are the variable fusion line profile, depth of

penetration and width of the dissimilar transition zone generated by the first layer, and the depth of penetration of the second layer. As can be seen in Figures 11 and 12, these factors affect the HAZ tempering profile. A wider compositional transition zone would slow the heat transfer between the weld metal and the HAZ due to the shallower gradient of thermo-physical properties with the Alloy 625 filler metal having significantly higher thermal capacity and lower thermal conductivity compared to the low alloy steel base metal [7].

4. CONCLUSIONS

This study contributed to a better understanding of factors controlling the tempering response and tempering efficiency of weld overlays. The tempering response and tempering efficiency quantification approaches developed at The Ohio State University were experimentally validated.

The effects of the heat input, of the fusion boundary profile, tempering from subsequent beads, and width of the dissimilar transition zone in the first layer, and the depth of penetration of the second layer on the extent of HAZ tempering were demonstrated. These factors have complex interaction and their effect on the HAZ tempering response could only be evaluated and optimized using a comprehensive computational modeling approach.

As demonstrated by the results of this study, an optimized temper bead welding procedure would provide tempering by adjacent beads in the first layer, while avoiding re-austenitization and generating maximum number of tempering reheats in the subsequent layers.

REFERENCES

[1] Lippold, John C., *Welding Metallurgy and Weldability.* John Wiley & Sons, 2014.

[2] L. Yu, et al., "Neural Network Prediction of Hardness in HAZ of Temper Bead Welding Using the Proposed Thermal Cycle Tempering Parameter (TCTP)," ISIJ Int., vol. 51, no. 9, pp. 1506–1515, 2011..

[3] ASME. Boiler and Pressure Vessel Code (BPVC), Section IX, QW-290, *Temper Bead Welding*, 2019 Edition.

[4] Stewart J. and Alexandrov B.T., 2020. Quantification of the Tempering Response in the Heat-affected Zone of Low Alloy Steels Subjected to Temper Bead Welding. Submitted for journal publication in February, 2020.

[5] Stewart, Jeffrey, *Temper Bead Welding for Dissimilar Metal Welds and Overlays.* 2019. The Ohio State University, PhD Dissertation.

[6] Forquer, Matt, *Simplified Computational Modeling Approach for Analysis and Optimization of Temperbead Welding Procedures*. 2018. Ohio State University, MSc thesis.

[7] Kuper, M.W. and B.T. Alexandrov, 2019. Retention of Delta Ferrite in the Heat Affected Zone of Grade 91 Steel Dissimilar Metal Welds. **Materials and Metallurgical Transactions A**, **50A**, pp. 2732-2747.